International Journal of Hydrogen Energy 85 (2024) 625–634

Contents lists available at ScienceDirect

International Journal of Hydrogen Energy

journal homepage: www.elsevier.com/locate/he

Assessment of a NaOH-based alkaline electrolyser's performance: System modelling and operating parameters optimisation

Francesca Mennilli [a], Lingkang Jin [b], Mosè Rossi [a,*], Gabriele Comodi [a]

[a] Marche Polytechnic University, Department of Industrial Engineering and Mathematical Sciences (DIISM), Via Brecce Bianche, 12, Ancona, 60131, Italy
[b] Eindhoven University of Technology, Department of Electrical Engineering, Electrical Energy Systems, Eindhoven, 5600 MB, The Netherlands

ARTICLE INFO

Keywords:
Alkaline electrolyser
Electrochemical parameters fitting
NaOH-based electrolyte
Optimisation procedure
Sensitivity analysis

ABSTRACT

Most of the scientific research is focused on KOH-based alkaline electrolysers, while NaOH-based ones are unexplored although they present interesting features. This paper presents a semi-empirical model developed in the Python environment to predict a NaOH-based alkaline electrolyser's performance to cover such a research gap and perform an optimisation procedure of electrochemical parameters. A sensitivity analysis has been carried out to study how its performance changes while varying the: i) NaOH content, ii) pressure, and iii) both. Separately, the best result has been obtained with a NaOH content and an operating pressure of 8% and 6.5 bar, respectively. Furthermore, the same values have been recorded even by varying both the NaOH content and the operating pressure. Specifically, a maximum average efficiency increase of 3.57% at 35 °C, 0.17% at 40 °C, and 3.74% at 35 °C in the case of NaOH content, pressure, and both, respectively.

1. Introduction

The ever-increasing global energy demand and population growth in the past decades led to an over-exploitation of fossil fuels and thus climate change issues that are currently undergoing and affecting human beings that live on Earth. The United Nations Environment Programme (UNEP) stated that the coal, oil & gas production from government plans & projections will increase up to 2030 and 2050, respectively, being still far away from both the 0.5 and 2°C-consistent pathlines [1]. That said, a fast and progressive transition to clean and reliable energy sources is mandatory and urgently required for addressing these issues.

In such a context, water electrolysis is considered one of the possible solutions to speed up the decarbonisation process as reported by [2], where the authors provided a recent review and evaluation of this electro-chemical process from different environmental and techno-economic aspects such as hydrogen cost production, electrode materials development, etc. In particular, if coupled with Renewable Energy Sources (RESs) water electrolysers produce the so-called green hydrogen to be used either as energy vector, or storage means in medium-long term periods to provide grid stability as other energy storage systems like batteries [3].

Several electrolysis technologies are currently available in the global market. In particular, Alkaline, Proton Exchange Membrane (PEM), Solid Oxide (SO), and Molten Carbonate (MC) electrolysers are the most widespread at both the industrial and residential levels as well as at laboratory scales, while the Anion Exchange Membrane (AEM) technology is still under development [4].

Among the above-mentioned technologies, the Alkaline one is the most mature and widespread technology that is being currently used in different applications of the renewable energy sector [5]; indeed, Alkaline electrolysers have several advantages [6]:

- low cost due to the use of cheaper catalyst materials such as Nickel (Ni);
- high lifetime and gas purity;
- high operating pressure (up to 200 bar);
- high hydrogen production capacity (up to 3880 Nm^3/h); and
- low specific energy consumption (around 3.8 kWh/Nm^3).

However, if compared with other technologies, Alkaline electrolysers present:

- corrosion issues due to the alkaline solution, while PEM, AEM, and SO technologies use a solid/non-corrosive electrolyte which prevent them from a more frequent maintenance;
- low current density (e.g., 0.2–0.7 A/cm^2), while PEM and SO technologies can reach values up to 2 and 1 A/cm^2, respectively [6,7];
- non-compact design due to the low operating current density; and
- low efficiency (< 77%), while PEM and SO can reach values up to 83 and 90%, respectively [6,8].

* Corresponding author.
E-mail address: mose.rossi@staff.univpm.it (M. Rossi).

https://doi.org/10.1016/j.ijhydene.2024.08.175
Received 18 June 2024; Received in revised form 5 August 2024; Accepted 9 August 2024
Available online 28 August 2024

Nomenclature

Acronyms

AEM	Anion Exchange Membrane
CFD	Computational Fluid Dynamics
HER	Hydrogen Evolution Reaction
KOH	Potassium Hydroxide
MC	Molten Carbonate
MW	Molecular Weight
NaOH	Sodium Hydroxide
OCV	Open Circuit Voltage
OER	Oxygen Evolution Reaction
PEM	Proton Exchange Membrane
PPS	Polyphenylene Sulphide
RES	Renewable Energy Source
$RMSE$	Root Mean Square Error
SO	Solid Oxide
$UNEP$	United Nations Environment Programme
wtp	weight title percent

Physics constants

F	Faraday's constant (96,485 C/mol)
LHV	Lower Heating Value of hydrogen (120 MJ/kg)

Electrochemical variables

α	Charge transfer coefficient
δ	Membrane thickness (cm)
$\dot{m}_{H_2}$	Mass rate of hydrogen (kg/s)
$\dot{n}_{H_{2th}}$	Theoretical molar rate of hydrogen (mol/s)
$\dot{n}_{H_2}$	Molar rate of hydrogen (mol/s)
η	Electrolyser energy efficiency
η_f	Faraday efficiency
σ_{el}	Electrolyte solution conductivity (S/cm)
A_{an}	Anode area (cm^2)
A_{cat}	Cathode area (cm^2)
A_{cell}	Cell area (cm^2)
d_{as}	Distance anode - separator (cm)
d_{cs}	Distance cathode - separator (cm)
E_{OCV}	Open Circuit Voltage (V)
E_{rev}	Reversible potential (V)
i	Current density (A/cm^2)
i_0	Exchange current density (A/cm^2)
K_1	Empirical constant (S/m)
K_2	Empirical constant (S/m*°C)
K_3	Empirical constant (S/m)
K_4	Empirical constant (S/m)
K_5	Empirical constant (S/m)
n	Number of electrons exchanged (2)
N_c	Number of cells
P_{el}	Electric power consumption (W)
P_{el}	Partial pressure of electrolyte solution (Pa)
P_{H_2O}	Partial pressure of water vapour (Pa)
P_{H_2}	Partial pressure of hydrogen (Pa)
P_{N_aOH}	Partial pressure of electrolyte (Pa)
P_{O_2}	Partial pressure of oxygen (Pa)
R	Universal gas constant (J/mol K)
R_{el}	Electrolyte solution resistance
R_{sep}	Separator resistance
T	Cell temperature (K)
V	Cell potential (V)
$V_{act,a}$	Anode activation overpotential (V)
$V_{act,c}$	Cathode activation overpotential (V)
V_{ohm}	Ohmic overpotential (V)
x_{H_2O}	Molar fraction of water
x_{N_aOH}	Molar fraction of electrolyte

Alkaline electrolysers consist of multiple electrochemical cells, commonly arranged in series, where two electrodes are partially submerged in either Potassium Hydroxide (KOH)- or Sodium Hydroxide (NaOH)-based electrolyte. Water and electricity are supplied to the cell to initiate the electrolytic reaction, which splits the water molecules and produces hydrogen and oxygen according to Eqs. (1) (cathode reaction) and (2) (anode reaction), respectively:

$$2H_2O + 2e^- \longrightarrow 2OH^- + H_2 \quad (1)$$

$$2OH^- \longrightarrow (1/2)\,O_2 + H_2O + 2e^- \quad (2)$$

Most of the commercial alkaline electrolysers are KOH-based since they use non-noble catalysts (e.g., Nickel, Cobalt, Iron, etc.) to lower the activation energies and accelerate the reactions; as a consequence, they have been deeply studied by several scientists [9], particularly by means of numerical models to predict their performance at different operating conditions. Gilliam et al. [10] focused on specific conductivity data of aqueous KOH-based solutions. They proposed an empirical model, which is based on the density concentration, to compare experimental conductivity data obtained at fixed KOH weight percentage and molarity. The best correlation coefficient of 0.998 was obtained over a molarity range of 0–12 M at temperatures of 0 – 100 °C, showing its good accuracy capability over a broader concentration range with a maximum deviation of ± 6% and an average value of 1.5%. Artuso et al. [11] proposed an electrolyser's model that has been validated with real data of a 36 kW-alkaline technology. The electrolyser operated at rated conditions as well at different part-loads, namely at 60 and 20% of its rated power. Results showed that the model was able to correctly evaluate the overall hydrogen production, showing a maximum percentage error of 0.89%. Abdin et al. [12] developed a one-dimensional model of a KOH-based alkaline electrolyser, which is based on 7 free model parameters, to assess the influence of its components on the cell potential. They used parameters related to the materials and components configuration, obtaining a good match between numerical and real data.

However, the authors of the research works previously mentioned did not perform any optimisation procedures for tuning their model to better fit the experimental points, which is nowadays crucial for properly assessing the performance of this technology at different operating conditions. In this regard, Hammoudi et al. [13] presented a multi-physics model for designing alkaline electrolysers. The model allows to choose precisely the design parameters of an alkaline electrolyser to obtain targeted energy consumption, efficiency, and hydrogen production rate. The model has been validated with experimental tests on two different electrolysers having a power input of 5 and 26 kW, showing a deviation of 1.2 and 3% with an operating pressure of 10 and 30 bar at a temperature of 80 °C, respectively. Amores et al. [14] developed a mathematical model from the Ulleberg's equation to resemble the optimal operation of an alkaline water electrolyser for hydrogen production (e.g., polarisation curves). Results were validated with experimental data showing a very good accuracy; indeed, the maximum error was around 1% in all the analysed polarisation curves. DaCruz et al. [15]

proposed an optimisation model for a KOH-based alkaline electrolyser operating in transient conditions using orthogonal collocation on finite elements. The main goal was to minimise the operating costs of the electricity consumption while keeping the hydrogen yield constant. Results showed that it is possible to save up to 17% of the electricity costs compared to a constant plant capacity.

Nevertheless, the models described so far use 7, 11, and 17 variable parameters, respectively, related to the geometry of the electrolysers, operating pressure and temperature, materials, concentration, electrical conductivity, bubbling, the influence of both electrolyte concentration, distance between electrodes, hydrogen/electrolyte separator, and oxygen/electrolyte that are difficult to calculate since they require detailed characteristics either from alkaline electrolyser's manufacturers, or expensive lab equipment which is not always affordable. One option to perform a deep analysis on the electrolyser's behaviour is the use of Computational Fluid Dynamics (CFD)-based software. Indeed, Zarghami et al. [16] performed a CFD analysis of a water-based electrolyser to analyse the multiphase flow and compare the results, at different current densities, with experimental data. They added the turbulence dispersion force to the model and achieved a better agreement between numerical and real data, thus showing its important role in properly resembling the different operating conditions. Muhsen et al. [17] developed a CFD model and performed a parametric study with COMSOL© Multiphysics along with a sensitivity testing within specified parameter ranges. Results showed that the diaphragm porosity has a pivotal role in the electrolyser's efficiency, especially at 15 and 60%. In addition, the electrode–diaphragm gap trend has a nonlinear increase in the cell current density as the gap decreases from its average; consequently, a 75% decrease of the hydrogen yield over the rated current density is obtained. Liu et al. [18] proposed a 2D, non-isothermal multi-physical model with a two-phase flow, mass, heat, and charge transfer processes based on COMSOL© Multiphysics which has been validated with experimental data. Results showed a good alignment with the KOH-based alkaline electrolyser operating voltages between 323–343 K, and the relative percentage error was below 2.2% even at high current densities up to 1.5 A cm^2. The corresponding Hydrogen Evolution Reaction (HER) and Oxygen Evolution Reaction (OER) overpotentials of the porous electrodes showed a good accuracy as well; indeed, the temperature distribution and ionic species inside the porous electrodes at various volumetric flow rates and current densities has been correctly obtained. However, it should be highlighted that the use of commercial CFD software requires a greater computational effort than 0D or 1D models which are good enough for providing reliable results on the technology's performance.

After highlighting both the pros and cons of the research works discussed so far, it is worth noting that all of them are focused on the characterisation of KOH-based alkaline electrolysers, while there are a few research works on NaOH-based ones. In particular, NaOH-based electrolysers are worth to be investigated considering the following aspects:

- the use of a liquid solution based on a NaOH electrolyte offers a cheaper option than the KOH one due to lower production costs [6,19];
- a given concentration of the NaOH electrolyte that is about 35% more conductive than the same mass of the KOH. To increase the conductivity, a higher amount of the KOH electrolyte is needed with a further higher cost of the electrolyte as well [20];
- NaOH-based electrolytes tend to be less corrosive than the KOH-based ones, thus allowing to adopt cheaper materials (e.g., carbon steel, Nickel without cathodic protection) [21]; and
- reaction products such as iron dissolution, if it is present, from the KOH electrolyte is more soluble than those obtained with the NaOH one, which makes more difficult its removal afterwards [22].

Conversely, it must be also highlighted that:

- although the NaOH-based electrolyte is less corrosive than the KOH-based one, regular maintenance is always required to guarantee safe operations and good performance of the system [6];
- alkaline electrolysers manufacturers prefer to use a KOH electrolyte instead of a NaOH one since, for the same concentration of electrolyte, KOH has a higher specific conductivity at the standard operating temperature of the system (e.g., 50–80 °C) [6].

That said, to the authors' knowledge, optimisation procedures regarding the main electrochemical characteristics of the alkaline electrolysers along with a sensitivity analysis by investigating different operating conditions have not been deeply analysed so far. As a consequence, this technology is still not fully explored in terms of performance. The main contribution of the present work is to cover this research gap by developing a numerical model in the Python programming environment [23] to analyse and optimise the performance of a NaOH-based alkaline electrolyser installed at the Department of Industrial Engineering and Mathematical Sciences (DIISM) of the Marche Polytechnic University, Italy.

The paper is structured as follows: Section 2 provides characteristics and performance of the NaOH-base electrolyser under investigation. Section 3 provides a complete overview of the numerical model developed with a detailed description of the analysed case studies. Section 4 describes the fitting process performed to obtain some of the parameters required by the model to perform the simulations. Section 5 shows and discusses the results, highlighting the operating conditions that optimise the overall system. Finally, Section 6 reports the conclusions of the work and its possible future developments.

2. Alkaline electrolyser's performance

This section presents both the alkaline electrolyser's characteristics and performance obtained in the experimental campaign. Precisely, the technical characteristics of the analysed electrolyser are listed in Table 1, while the system's performance is shown in Figs. 1 and 2 in terms of polarisation curves, which is the main curve to analyse the behaviour of this technology.

Table 1
Investigated alkaline electrolyser's characteristics.

Feature	Value
Rated power (kW)	23
Number of cells	160
Cell area (cm^2)	450
Weight title of electrolyte (NaOH)	0.18
Cell operating pressure (bar)	4.5
Cell operating temperature (°C)	25–55
Electrode materials	Carbon steel (no catalysts)
Distance electrode–diaphragm (cm)	0.3
Electrodes thickness (cm)	0.1
Electrodes area (cm^2)	580
Diaphragm material	PPS
Diaphragm thickness (cm)	0.1
Diaphragm area (cm^2)	580

As reported by Fig. 1, only data up to a cell temperature of 40 °C were available since the electrolyser has not been explored under full load conditions yet. Fig. 2 displays experimental points obtained at a hydrogen pressure of 4.5 bar with a lower cell potential than the points at lower pressures; this is particularly evident from data collected at gas pressures ranging from 0 (system start-up) to 3 bar. This behaviour is due to the operating conditions and materials used in the analysed technology (see Table 1). More details are reported in Section 5.

Furthermore, most of the experimental data are collected at a hydrogen pressure of 4.5 bar because the analysed electrolyser reaches this operating pressure within 10 minutes of the start-up phase, while the temperature takes a longer time to rise up and then stabilise. This means that (i) there are few experimental data at gas pressures lower

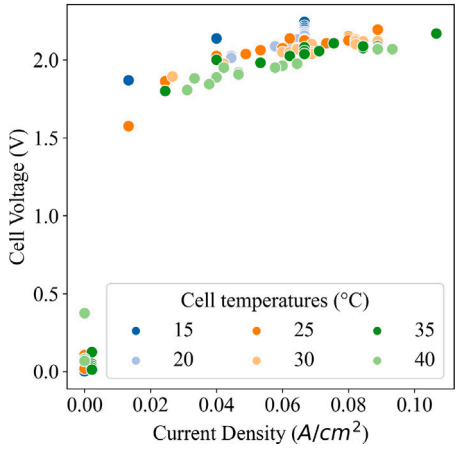

Fig. 1. Experimental points at different cell operating temperatures.

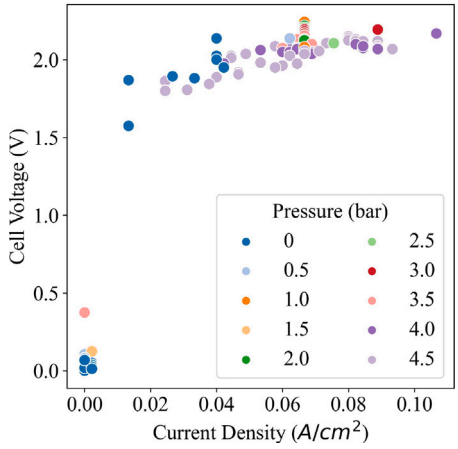

Fig. 2. Experimental points at different hydrogen pressures.

than 4.5 bar, and (ii) there is no correspondence between the increase of both the operating pressure and temperature of the electrolyser.

It is worth noting that no experimental data have been collected in the activation region of the polarisation curves; indeed, when the electrolyser starts operating, there is a sudden increase in the absorbed electric current that directly leads the cells to operate in the ohmic region. As a consequence, it is not possible to record the system's behaviour in the activation zone.

3. Materials and methods

In this section, a detailed description of the Python semi-empirical model and case studies are reported.

3.1. Electrolyser's semi-empirical model

A semi-empirical model has been developed in the Python programming environment which uses mathematical relations reported in the scientific literature. The model has been validated with the experimental data of a NaOH-based alkaline electrolyser (see Section 2) installed at the Department of Industrial Engineering and Mathematical Sciences (DIISM) of the Marche Polytechnic University, Italy. The main performance curve of an electrolyser is the polarisation one that represents the relationship between the current density and the cell potential as expressed by Eq. (3):

$$V = N_c \cdot (E_{OCV} + V_{act,a} + V_{act,c} + V_{ohm} + V_{conc}) \tag{3}$$

where N_c is the number of electrolyser cells, E_{OCV} (V) is the Open Circuit Voltage, $V_{act,a}$ (V) and $V_{act,c}$ (V) are the anode and cathode activation overpotentials, respectively, V_{ohm} (V) is the Ohmic overpotential, and V_{conc} is the concentration overpotential. The latter occurs at high current densities when the reaction rate is slowed down by the overpopulation of reacting molecules. In this case, the concentration losses have been neglected as the experimental tests have been performed without entering this region of the polarisation curve, thus keeping the current density low. The OCV is obtained through the Nernst's equation according to [24]:

$$E_{OCV} = E_{rev} + \frac{R \cdot T}{n \cdot F} ln \frac{P_{H_2} \cdot P_{O_2}^{0.5}}{P_{el}} \tag{4}$$

where P (Pa) is the partial pressure of reactants/products, T (K) is the cell temperature, F (C/mol) is the Faraday's constant, R (J/molK) is the universal gas constant, and E_{rev} (V) is the reversible cell potential that is calculated using Eq. (5) from [24]:

$$E_{rev} = 1.229 - 0.910^{-3} \cdot (T - 298) \tag{5}$$

The partial pressure of the electrolyte solution P_{el} has been calculated assuming an ideal behaviour of the solution according to Raoult's law [25] as reported in Eq. (6):

$$P_{el} = P_{H_2O} \cdot x_{H_2O} + P_{N_aOH} \cdot x_{N_aOH} \tag{6}$$

In this case, the contribution of the electrolyte has been neglected being less volatile and contained in a low volume percentage concentration in the water. As a consequence, the Raoult's law for a solution with low volatile solute is written as reported in Eq. (7):

$$P_{el} = P_{H_2O} \cdot (1 - x_{N_aOH}) \tag{7}$$

Regarding the activation overpotential calculation, a simplified expression based on the Butler–Volmer's equation, which is the so-called Tafel's one, is used for both the anode and cathode like in [26]:

$$V_{act,x} = \frac{R \cdot T}{n \cdot F \cdot \alpha_x} \cdot ln \frac{i}{i_{0,x}} \tag{8}$$

where α_x (dimensionless) is the charge transfer coefficient of the anode or cathode, i (A/cm^2) is the current density, and $i_{0,x}$ (A/cm^2) is the exchange current density of the anode or cathode.

It is worth noting that the charge transfer coefficient has been assumed equal to 0.5 for both electrodes, while the exchange current density is calculated as a function of the Arrhenius' law and the composition of reacting gases [27] by knowing the reference exchange current density of both the anode and cathode $i_{0x,ref}$ (A/cm^2) along with their activation energy $E_{act,x}$ (J/mol) as shown in Eqs. (9) and (10), respectively:

$$i_{0,cat} = i_{0cat,ref} \cdot \left(\frac{P_{H_2}}{P_{ref}}\right) \cdot \left(\frac{P_{el}}{P_{ref}}\right)^{0.25} \cdot exp\left(\frac{-E_{act,cat}}{R \cdot T}\right) \tag{9}$$

$$i_{0,an} = i_{0an,ref} \cdot \left(\frac{P_{O_2}}{P_{ref}}\right) \quad exp \cdot \left(\frac{-E_{act,an}}{R \cdot T}\right) \tag{10}$$

where P_{ref} is the reference pressure of the system (e.g., atmospheric), $i_{0cat,ref}$ and $i_{0an,ref}$ are the cathode and anode reference exchange current densities, respectively, and $E_{act,cat}$ and $E_{act,an}$ are the cathode and anode's reaction activation energies, respectively. In this study, activation energies and reference exchange current densities have been calculated with a fitting process (see Section 4).

The Ohmic losses are evaluated with the Ohm's law considering only the diaphragm and the electrolyte solution resistances since they are the predominant ones:

$$V_{ohm} = (R_{sep} + R_{el}) \cdot i \tag{11}$$

where R_{sep} $(\Omega * cm^2)$ and R_{el} $(\Omega * cm^2)$ are the separator and electrolyte solution resistances, respectively. The separator resistance is evaluated as in Eq. (12):

$$R_{sep} = \frac{\delta}{\sigma_{el}} \tag{12}$$

where δ (cm) is the separator thickness and σ_{el} (S/cm) is the electrolyte solution conductivity. The latter is calculated using the Le Bideau formula [20] as reported in Eq. (13):

$$\sigma_{el} = K_1 + K_2 \cdot T + K_3 \cdot wtp^3 + K_4 \cdot wtp^2 + K_5 \cdot wtp \tag{13}$$

where coefficients from K_1 to K_5 are empirical coefficients obtained from the fitting process (see Section 4), while wtp is the weight title percent of NaOH (see Table 1).

The electrolyte solution resistance is calculated considering the occupied space by the solution within the cell as reported in Eq. (14):

$$R_{el} = \left[\left(\frac{1}{\sigma_{el}}\right) \cdot \left(\left(\frac{d_{as}}{A_{an}}\right) + \left(\frac{d_{cs}}{A_{cat}}\right)\right)\right] \cdot A_{cell} \tag{14}$$

where A_{cell} (cm^2) is the cell active area, d_{as} (cm) and d_{cs} (cm) are the anode and cathode distance from the separator, respectively, and A_{an} (cm^2) and A_{cat} (cm^2) are the anode and cathode geometric areas, respectively (see Table 1). The hydrogen production rate is evaluated with the Faraday's law [28] as reported by Eq. (15):

$$\dot{n}_{\text{H}_2} = \frac{\eta_f \cdot i \cdot A_{cell} \cdot N_c}{n \cdot F} \tag{15}$$

where η_{f} is the Faraday's efficiency that is calculated according to Eq. (16):

$$\eta_f = \frac{\dot{n}_{\text{H}_2}}{\dot{n}_{\text{H}_2 th}} \tag{16}$$

where $\dot{\text{n}}_{\text{H}_2}$ (mol/s) is the effective hydrogen production and $\dot{\text{n}}_{\text{H}_2\text{th}}$ (mol/s) is the theoretical hydrogen production without parasitic losses. In this case, the calculated average Faraday's efficiency of the electrolyser is equal to 0.95. The electric power consumption is evaluated with Eq. (17):

$$P_{el} = V \cdot i \cdot A_{cell} \cdot N_c \tag{17}$$

and, finally, the energy efficiency (e.g., input electricity to feed the electrolyser for hydrogen production) is given by Eq. (18):

$$\eta = \frac{P_{out}}{P_{in}} = \frac{\dot{m}_{\text{H}_2} \cdot LHV}{P_{el}} \tag{18}$$

where $\dot{\text{m}}_{\text{H}_2}$ (kg/s) is the mass rate of hydrogen calculated according to Eq. (19):

$$\dot{m}_{\text{H}_2} = \dot{n}_{\text{H}_2} \cdot MW \tag{19}$$

where MW is the molecular weight of hydrogen (kg/mol).

3.2. Case studies

The developed semi-empirical model has been used to implement three case studies. Numerical simulations at different operating conditions in terms of pressure and electrolyte weight title have been performed to determine which of them allows to reach the maximum efficiency concerning the base operating conditions reported in Table 1.

The first case study involves the variation of the electrolyte content, while the second one involves the variation of the operating pressure. Finally, the third case study involves the variation of both the electrolyte weight title and cell pressure. In this way, benefits from each operating mode are assessed, choosing the one that better fits the system under investigation from a techno-economic point of view.

4. Fitting process of model parameters

As mentioned in Section 3, the reference exchange current densities are obtained through a curve-fitting process performed in the Python programming environment per each set of operating conditions along with the activation energies and electrolyte solution conductivity empirical coefficients. The curve fitting process is performed using optimisation algorithms to find the parameters that best fit the real data.

In particular, the optimisation algorithm looks at the numerical values related to model parameters that minimise the sum of the squared differences between the observed data points and the corresponding ones predicted by the model [29]. The objective function to be minimised is the following:

$$\sum_{i=1}^{k} (y_i - f(x_i, p))^2 \tag{20}$$

where p is the parameter vector to be optimised, k the number of data points, x_{i} and y_{i} are the coordinates of the ith data points, and $f(x_{\text{i}}, p)$ is the model prediction given the parameter vector p. It is worth noting that a proper range of variation of the resulting coefficients has to be set to avoid unrealistic values.

In this case, the electrolyte solution empirical coefficients range has been chosen considering the values reported in the scientific literature [20], while a wide range of variation for the exchange current densities and activation energies has been chosen to contain a large number of optimal values [30]. The ranges of variations are reported in Table 2 per each condition of cell temperature along with the fitted parameters.

An initial fitting process is performed at 25 °C and 4.5 bar from which reference exchange current densities, activation energies, and electrolyte empirical coefficients reported in Table 2 are obtained. The fitting algorithm is successfully applied to the other temperatures by keeping the first four parameters constant for as long as possible while fitting only those related to the electrolyte. This is because kinetic parameters, such as exchange current densities and activation energies, are calculated as reference coefficients at a reference operating condition, which is the one at 25 °C and 4.5 bar. Once these values are obtained, they have been used as input to the other operating conditions by fitting only the coefficients related to the electrolyte. It is worth noting that the semi-empirical model calculates the exchange current density values per each operating condition through Arrhenius' law starting from the reference ones [27]. The developed model adapts the kinetic parameters at any temperature and pressure conditions by taking as input a single combination of reference values.

Regarding the coefficients related to the electrolyte, they have been fitted at each operating cell temperature to adapt the NaOH conductivity equation to the system under investigation. As a consequence, five mathematical relations have been derived through a non-linear regression technique to describe the behaviour of each parameter with the cell operating temperature:

$$K_1 = -0.22 \cdot T^3 + 22.057 \cdot T^2 - 716.52 \cdot T + 7,593.44 \tag{21}$$

$$K_2 = -0.00448 \cdot T^3 + 0.445 \cdot T^2 - 14.46 \cdot T + 154.647 \tag{22}$$

$$K_3 = -1.92 \cdot 10^{-}7 \cdot T^3 + 1.88 \cdot 10^{-}5 \cdot T^2 - 0.00061 \cdot T + 0.00657 \tag{23}$$

$$K_4 = 3.43 \cdot T^3 - 318.057 \cdot T^2 + 9,455.77 \cdot T - 92,156.29 \tag{24}$$

$$K_5 = 1.38 \cdot T^3 - 141.15 \cdot T^2 + 4,736.37 \cdot T - 51,643.29 \tag{25}$$

With the above mathematical relations, along with the fitted parameters reported in Table 2, the electrolyser's behaviour at operating conditions that have not been tested is obtained, thus allowing for saving time and economic expenses. As previously mentioned, three case studies have been considered by simulating the system's performance at different conditions of the NaOH content and cell pressure to target the optimal ones from an efficiency point of view.

Table 2
Coefficients obtained from the fitting process.

	Range of variation	Fitted values at 25 °C	Fitted values at 30 °C	Fitted values at 35 °C	Fitted values at 40 °C	Unit of measure
$i_{0an,ref}$	(0.000001–0)	0.000564	–	–	–	A/cm^2
$i_{0cat,ref}$	(0.000001–0)	0.0000162	–	–	–	A/cm^2
$E_{act,an}$	(0–100,000)	22,409	–	–	–	J/mol
$E_{act,cat}$	(0–150,000)	66,494	–	–	–	J/mol
K_1	(-60-0)	−8.89	−55.66	−0.425	−9.9966	S/m
K_2	(0–2)	1.22	0.34	1.55	1.4878	S/m ° C
K_3	(0.000001–0)	0.000082	0.000027	0.0000502	0.000007548	S/m
K_4	(4000-0)	−882.21	−2000.56	−3566.089	−3002.85	S/m
K_5	(0–800)	130.06	709.03	447.14	380.55	S/m

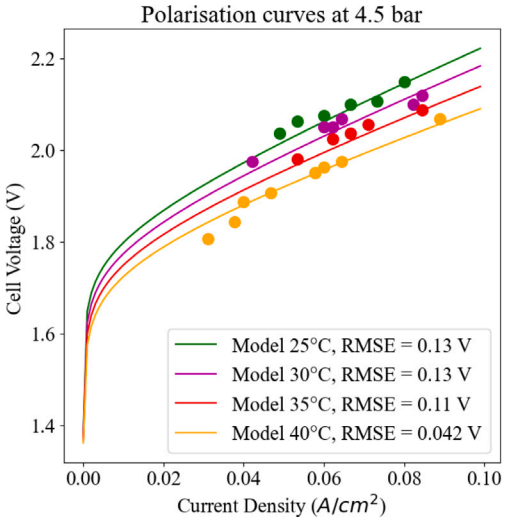

Fig. 3. Model validation at different cell temperatures while the pressure is fixed at 4.5 bar. (For interpretation of the references to colour in this figure legend, the reader is referred to the web version of this article.)

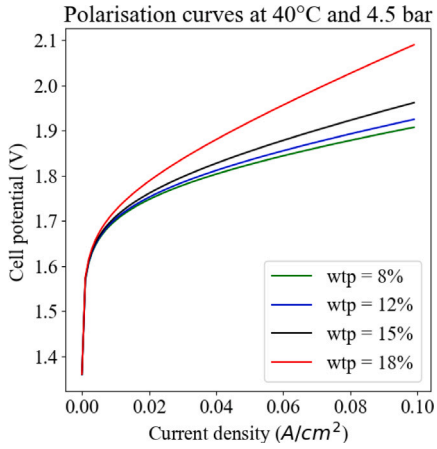

Fig. 4. Simulated polarisation curves at different electrolyte weight title percent. The cell operating temperature and pressure are 40 °C and 4.5 bar, respectively. (For interpretation of the references to colour in this figure legend, the reader is referred to the web version of this article.)

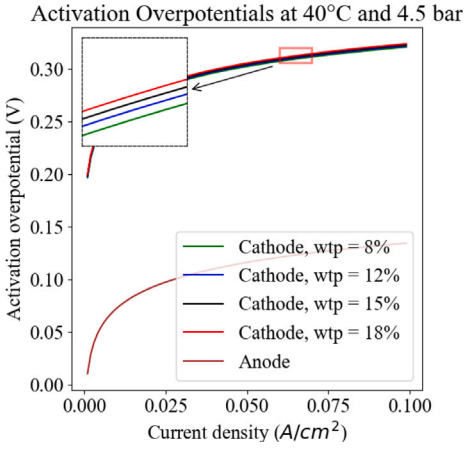

Fig. 5. Electrodes activation overpotentials at different electrolyte weight title percent. The cell operating temperature and pressure are 40 °C and 4.5 bar, respectively.

5. Results and comments

The semi-empirical model described in Section 3 has been validated with experimental data obtained from the alkaline electrolyser installed at the Marche Polytechnic University, Italy, whose characteristics are reported in Table 1. Data were recorded at cell temperatures ranging from 25 °C (green points) to 40 °C (orange points) and at a fixed operating pressure of 4.5 bar.

Fig. 3 shows the validation of the numerical model; as it can be noticed, polarisation curves are coherent with the scientific theory and the recorded maximum value of the Root Mean Square Error (RMSE) is 0.13 V at 25 °C and 30 °C. The model is then considered reliable and used for subsequent analysis.

5.1. First case study: variation of weight title percent of NaOH

In this case, the weight title percent (wtp) of electrolyte has been varied between 8 and 25%, being coherent with a range of validity of Le Bideau relation for the electrolyte conductivity [20]. Fig. 4 shows the polarisation curves simulated at different conditions of the electrolyte wtp, at a cell operating temperature and pressure of 40 °C and 4.5 bar, respectively. It is worth noting that simulation results at NaOH contents higher than 18% have not been considered in this case since an increase of the electrolyte wtp beyond this value leads to a negative ionic conductivity of the latter. From a physical point of view, this can be related to an excess of free ions that globally worsens the performance of the electrolyte itself; indeed, although the conductivity of a solution increases with the ion concentration, some exceptions arise for highly concentrated solutions (e.g., NaOH or Sulphuric Acid solutions) where there is a maximum ion concentration beyond which the conductivity worsens. This might be due to an overpopulation of free ions within the solution hinders their movement, thus worsening the quality of the electrolyte in terms of ionic conductivity.

As it can be noticed, a wtp of 8% represents the best operating condition for this case; indeed, the corresponding polarisation curve (green curve) highlights, for the same current density, a lower cell potential compared to the others.

This means that, for the same amount of produced hydrogen, the electrolyser consumes less electric energy. As a consequence, its efficiency improves. Fig. 5 shows the anode and cathode activation

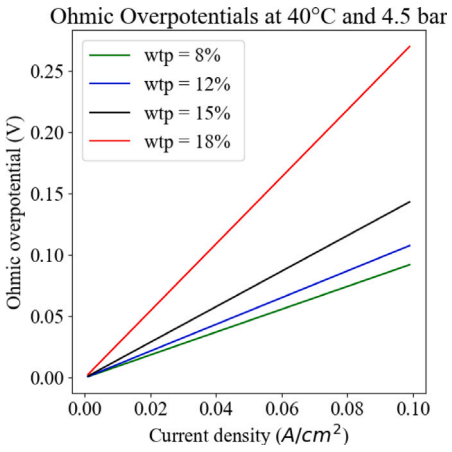

Fig. 6. Ohmic overpotentials at different electrolyte weight title percent. The cell operating temperature and pressure are 40 °C and 4.5 bar, respectively.

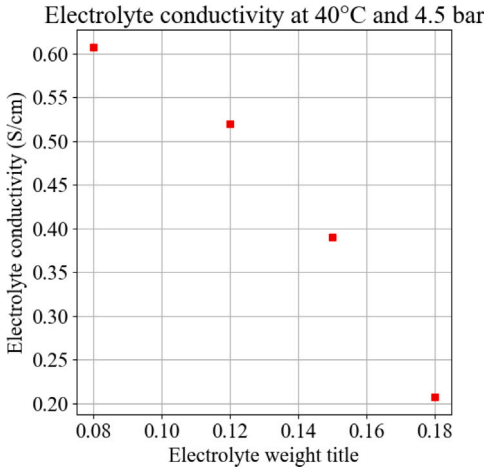

Fig. 7. Potassium Hydroxide conductivity. The cell operating temperature and pressure are 40 °C and 4.5 bar, respectively.

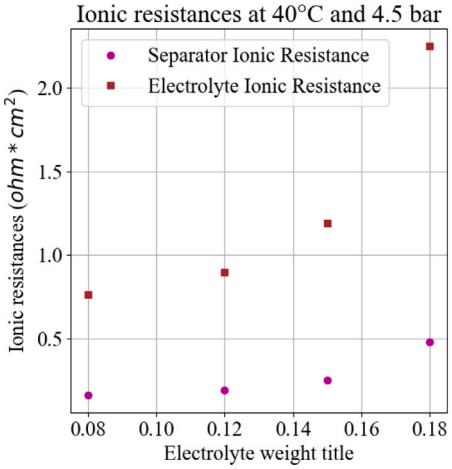

Fig. 8. Separator and electrolyte ionic resistances. The cell operating temperature and pressure are 40 °C and 4.5 bar, respectively.

overpotentials variation within the simulated electrolyte conductivity range. As can be noticed, only the cathode electrode is affected by the variation of the NaOH wtp since the electrolyte solution circulates towards the cathode side. Furthermore, the cathode activation

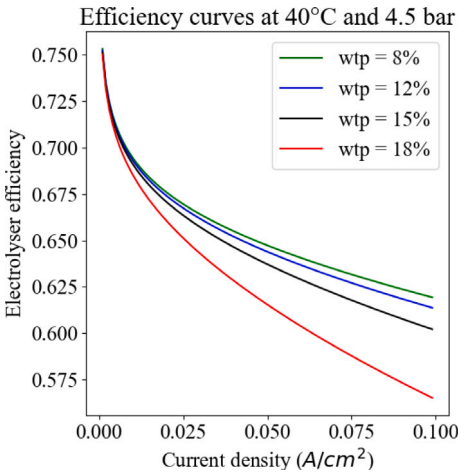

Fig. 9. Efficiency curves at different electrolyte weight title percent. The cell operating temperature and pressure are 40 °C and 4.5 bar, respectively.

overpotential is higher than the anode one, and it increases with the increase of the NaOH content. This is because, on the cathode side, water molecules must be split to generate gaseous hydrogen and OH^- ions, while on the anode side, simple recombination of ions and electrons occurs to generate gaseous oxygen. This means that the cathodic reaction is more expensive from an energy point of view than the anodic one and involves higher losses.

Fig. 6 shows the ohmic overpotentials at different conditions of electrolyte weight title percent. As it can be noticed, the curve corresponding to a NaOH content of 8% is the one with lower ohmic losses. This is because the electrolyte has a maximum ionic conductivity of 0.6 S/cm in this condition as shown in Fig. 7. Fig. 8 shows the separator and electrolyte ionic resistances at different NaOH contents. As it can be noticed, the separator becomes an ionic transport medium when its pores are filled with the electrolytic solution, thus the minimum resistance is reached with a wtp of 8%. Fig. 9 shows the efficiency curves of the electrolyser at different NaOH contents. As expected, the higher efficiency corresponds to a wtp of 8%, highlighting that this is the optimal operating condition for the electrolyser. Table 3 shows the optimal NaOH content, along with the percentage increase of average efficiency, concerning the efficiency obtained at the standard operating conditions reported in Table 1.

As it can be noticed, the optimal NaOH content is fixed at a value of 8% for all the temperatures except for 30 °C at which the resulting average efficiency is the lowest compared to the others. As a result, the electrolyte content variation improves the performance of the electrolyser with a maximum average efficiency increase of 3.57% at 35 °C.

5.2. Second case study: variation of operating pressure

As mentioned in Section 3, the alkaline electrolyser under investigation shows a performance improvement as the operating pressure increases. In this case, the maximum pressure was equal to 6.5 bar where issues related to the mechanical resistance and tightness of cell components at pressures much higher than the design one are considered (see Table 1). Fig. 10 shows the electrolyser polarisation curves at different operating pressures. As it can be noticed, the cell losses decrease from 2.5 to 6.5 bar, confirming that the system improves its performance while operating at higher pressures.

This is due to the decrease of the activation overpotential which has, in this case, a predominant effect on the increase of the open circuit voltage; indeed, there is an average reduction/increment of 4

Table 3
Optimal values of NaOH contents at each operating cell temperature.

Cell temperature (°C)	Optimal NaOH content (%)	Efficiency with NaOH wtp = 18% (%)	Efficiency with optimal NaOH content (%)	Average efficiency increase (%)
25	8	59.27	61.26	1.99
30	18	60.17	60.17	0
35	8	61.2	64.77	3.57
40	8	62.31	65.4	3.09

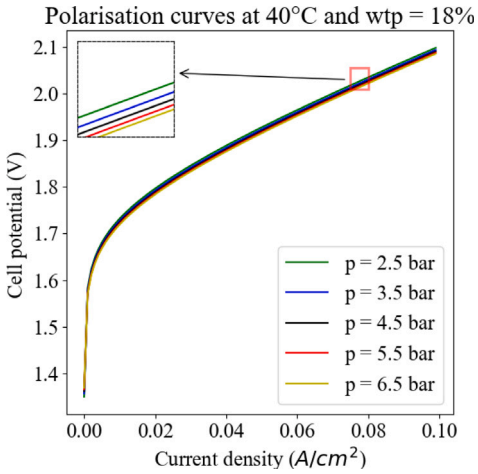

Fig. 10. Polarisation curves at different operating pressures. The cell operating temperature and NaOH content are 40 °C and 18%, respectively.

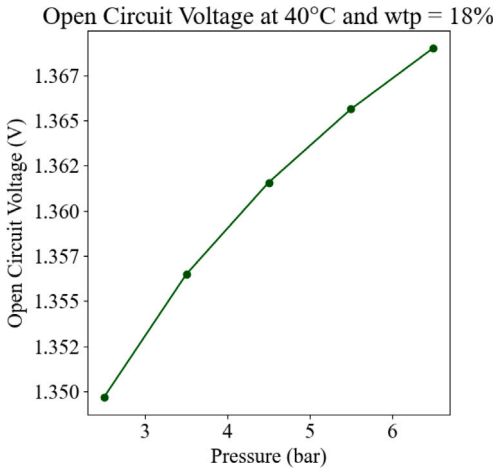

Fig. 12. Open circuit voltage variation with operating pressure. The cell operating temperature and NaOH content are 40 °C and 18%, respectively.

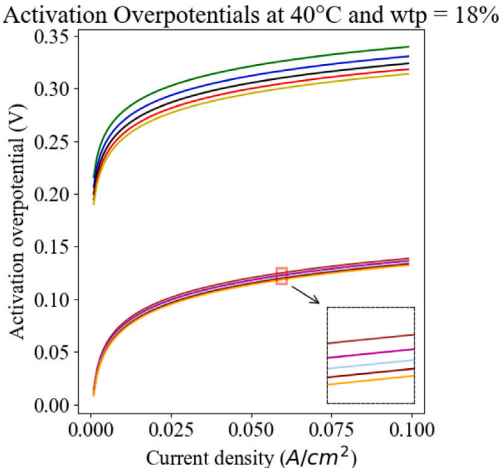

Fig. 11. Activation overpotentials at different operating pressures. The cell operating temperature and NaOH content are 40 °C and 18%, respectively. (For interpretation of the references to colour in this figure legend, the reader is referred to the web version of this article.)

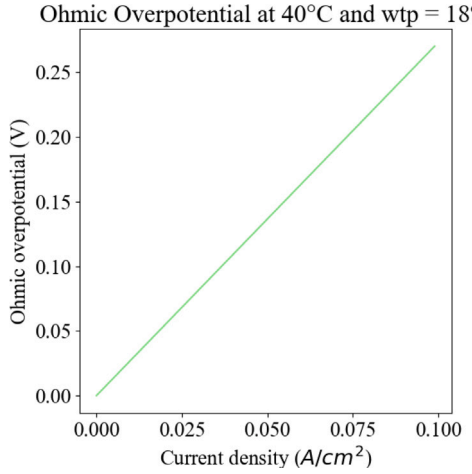

Fig. 13. Ohmic overpotential trend. The cell operating temperature and NaOH content are 40 °C and 18%, respectively.

and 2% of the overall activation overpotential and open circuit voltage, respectively. Trend details are shown in Figs. 11 and 12. It is worth noting that, in Fig. 11, curves from dark green to light green are related to the cathode activation overpotential simulated between 2.5 and 6.5 bar with a step of 1 bar. The same has been done for curves going from brown to orange, which are associated with the anode overpotential instead. The ohmic overpotential is not affected by the variation of operating pressure; indeed, there is a single trend throughout the pressure range simulated as shown in Fig. 13.

Finally, the electrolyser's efficiency curves at different pressures are displayed in Fig. 14. As it can be noticed, different pressure values have been considered, thus providing a wide overview of the electrolyser's performance. In particular, the following efficiencies recorded at the rated current density of 0.1 A/cm^2 have been obtained: namely, 56.3% at 2.5 bar, 56.4% at 3.5 bar, 56.5% at 4.5 bar, 56.6% at 5.5 bar, and 56.65% at 6.5 bar.

As a result, the higher efficiency is reached at a cell pressure of 6.5 bar, highlighting that this condition is beneficial for the system under investigation. Table 4 shows the optimal operating pressure, along with the percentage increase of average efficiency, concerning the efficiency obtained at standard operating conditions reported in Table 1.

As it can be noticed, the optimal pressure per each cell operating temperature is 6.5 bar, allowing to have a maximum average efficiency increase of 0.17% at 40 °C.

Table 4
Optimal values of pressure per each operating cell temperature.

Cell temperature (°C)	Optimal pressure (bar)	Efficiency at 4.5 bar	Efficiency with optimal pressure (%)	Average efficiency increase (%)
25	6.5	59.27	59.42	0.15
30	6.5	60.17	60.32	0.15
35	6.5	61.2	61.36	0.16
40	6.5	62.31	62.48	0.17

Table 5
Optimal pressure and NaOH content for each operating cell temperature.

Cell temperature (°C)	Optimal wtp (%)	Optimal pressure (bar)	Efficiency at standard operating conditions (%)	Efficiency at optimal operating conditions (%)	Average efficiency increase (%)
25	8	6.5	59.27	61.41	2.14
30	18	6.5	60.17	60.32	0.15
35	8	6.5	61.2	64.94	3.74
40	8	6.5	62.31	65.24	2.93

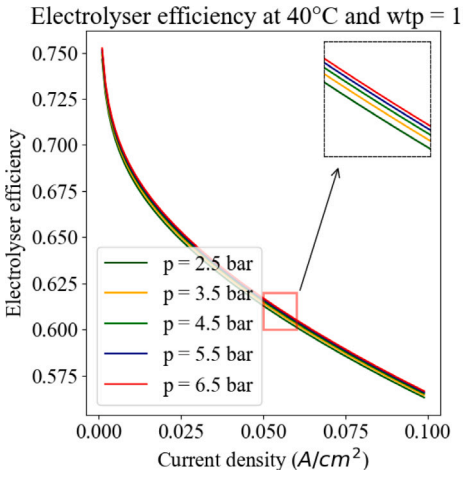

Fig. 14. Efficiency curves at different operating pressures. The cell operating temperature and NaOH content are 40 °C and 18%, respectively.

5.3. Third case study: variation of pressure and NaOH content

In this case, both the pressure and NaOH content have been varied to obtain the optimal combination of operating conditions that allow reaching the maximum efficiency of the electrolyser under investigation. Eq. (26) shows the mathematical condition to be satisfied:

$$max(\eta_{(wtp_{opt},p_{opt})} - \eta_{(wtp_{std},p_{std})}) \quad (26)$$

where wtp_{opt} and p_{opt} are the optimal values of NaOH content and pressure that maximise the efficiency, while wtp_{std} and p_{std} are referred to the current operating conditions of the electrolyser. Table 5 shows the optimal operating conditions that, per each cell operating temperature, allow to reach the maximum efficiency along with the average efficiency increase.

As expected, the optimal combination is obtained per each temperature by coupling the values identified in the previous case studies. Surely, if a control system for varying the operating conditions is installed, it will be possible to choose whether to manage only the NaOH content, the pressure level, or both based on techno-economic considerations.

Finally, the variation of both pressure and NaOH content improves the performance of the electrolyser under investigation, thus allowing to obtain a maximum average efficiency increase of 3.74% at 35 °C.

6. Conclusions

This work aims to provide insights into a NaOH-based electrolyte alkaline electrolyser technology. A semi-empirical model was developed in the Python programming environment to resemble and predict the behaviour of a 23 kW NaOH-based alkaline electrolyser installed at the Marche Polytechnic University, Italy.

Three case studies have been analysed, aiming to evaluate the optimal operating conditions that allow maximising the electrolyser's efficiency; in particular, the variation of NaOH content, pressure, and both have been considered.

Results showed that, in the case of weight title percent of electrolyte variation, the system's performance improves per each cell operating temperature, obtaining a maximum average efficiency increase of 3.57% at 35 °C.

In the second case study, which involves the operating pressure variation, it has been found that a pressure of 6.5 bar represents the optimal condition, obtaining a maximum average efficiency increase of 0.17% at 40 °C; indeed, considering a current density equal to the rated one, the efficiency curve at 6.5 bar is the highest, highlighting that this condition is beneficial for the system under investigation.

Variation of both pressure and NaOH content allowed to improve the electrolyser's performance at each cell operating temperature, obtaining a maximum average efficiency increase of 3.74% at 35 °C.

In all three case studies, it is possible to optimise the electrolyser's performance by improving its operation if a NaOH content or/and a pressure system control is implemented. The choice of the latter depends on techno-economic factors.

Further development of this work will involve a proper experimental campaign to evaluate the system's limits from an electrochemical point of view along with the implementation of a control system of the electrolyser's operating conditions.

CRediT authorship contribution statement

Francesca Mennilli: Writing – review & editing, Writing – original draft, Visualization, Software, Methodology, Investigation, Formal analysis, Data curation, Conceptualization. **Lingkang Jin:** Writing – review & editing, Writing – original draft, Visualization, Investigation, Formal analysis, Data curation. **Mosè Rossi:** Writing – review & editing, Writing – original draft, Visualization, Supervision, Formal analysis, Data curation. **Gabriele Comodi:** Writing – review & editing, Writing – original draft, Supervision, Resources, Formal analysis.

Declaration of competing interest

The authors declare that they have no known competing financial interests or personal relationships that could have appeared to influence the work reported in this paper.

References

[1] United Nations Environment Programme (UNEP). Production Gap Report 2023, https://productiongap.org/wp-content/uploads/2023/11/PGR2023_web_rev.pdf.

[2] Hassan N, Jalil A, Rajendran S, Khusnun N, Bahari M, Johari A, et al. Recent review and evaluation of green hydrogen production via water electrolysis for a sustainable and clean energy society. Int J Hydrog Energy 2024;52(Part B):420–41. http://dx.doi.org/10.1016/j.ijhydene.2023.09.068.

[3] Irham A, Roslan M, Jern KP, Hannan M, Mahlia TI. Hydrogen energy storage integrated grid: A bibliometric analysis for sustainable energy production. Int J Hydrog Energy 2024;63:1044–87. http://dx.doi.org/10.1016/j.ijhydene.2024.03.235.

[4] Titheridge L, Marshall A. Techno-economic modelling of AEM electrolysis systems to identify ideal current density and aspects requiring further research. Int J Hydrog Energy 2024;49:518–32. http://dx.doi.org/10.1016/j.ijhydene.2023.08.181.

[5] Hassan Q, Sameen A, Salman H, Jaszczur M. Large-scale green hydrogen production via alkaline water electrolysis using solar and wind energy. Int J Hydrog Energy 2023;48(88):34299–315. http://dx.doi.org/10.1016/j.ijhydene.2023.05.126.

[6] Gambou F, Guilbert D, Zasadzinski M, Rafaralahy H. A comprehensive survey of alkaline electrolyzer modeling: Electrical domain and specific electrolyte conductivity. Energies 2022;15(3452). http://dx.doi.org/10.3390/en15093452.

[7] David M, Ocampo-Martinez C, Sànchez-Pena R. Advances in alkaline water electrolyzers: A review. J Energy Storage 2019;23:392–403. http://dx.doi.org/10.1016/j.est.2019.03.001.

[8] Kim S, Kim T, Oh S, Ham J, Kang S. Numerical analysis of a solid oxide fuel cell system integrated with a hybrid desiccant cooling system. Energy Convers Manage 2023;296:117699. http://dx.doi.org/10.1016/j.enconman.2023.117699.

[9] Emam A, Hamdan M, Abu-Nabah B, Elnajjar E. A review on recent trends, challenges, and innovations in alkaline water electrolysis. Int J Hydrog Energy 2024;64:599–625. http://dx.doi.org/10.1016/j.ijhydene.2024.03.238.

[10] Gilliam R, Graydon J, Kirk D, Thorpe S. A review of specific conductivities of potassium hydroxide solutions for various concentrations and temperatures. Int J Hydrog Energy 2007;32(3):359–64. http://dx.doi.org/10.1016/j.ijhydene.2006.10.062.

[11] Artuso P, Gammon R, Orecchini F, Watson S. Alkaline electrolysers: Model and real data analysis. Int J Hydrog Energy 2011;36:7956–62. http://dx.doi.org/10.1016/j.ijhydene.2011.01.094.

[12] Abdin Z, Webb C, Gray EM. Modelling and simulation of an alkaline electrolyser cell. Energy 2017;138:316–31. http://dx.doi.org/10.1016/j.energy.2017.07.053.

[13] Hammoudi M, Henao C, Agbossou K, Dubé Y, Doumbia M. New multi-physics approach for modelling and design of alkaline electrolyzers. Int J Hydrog Energy 2012;37(19):13895–913. http://dx.doi.org/10.1016/j.ijhydene.2012.07.015.

[14] Amores E, Rodriguez J, Carreras C. Influence of operation parameters in the modeling of alkaline water electrolyzers for hydrogen production. Int J Hydrog Energy 2014;39(25):13063–78. http://dx.doi.org/10.1016/j.ijhydene.2014.07.001.

[15] da Cruz HMA, Etancelin M, Marias F, Reneaume J, Sochard-Reneaume S, Serra S. Dynamic modelling of an alkaline water electrolysis system and optimization of its operating parameters for hydrogen production. Int J Hydrog Energy 2023;48:12982–99. http://dx.doi.org/10.1016/j.ijhydene.2022.12.130.

[16] Zarghami A, Deen N, Vreman A. CFD modeling of multiphase flow in an alkaline water electrolyzer. Chem Eng Sci 2020;227:115926. http://dx.doi.org/10.1016/j.ces.2020.115926.

[17] Muhsen H, Alshawabkeh M, Al-Mahmodi M, Ghanem A, Al-Halhouli A. Sensitivity analysis of electrodes spacing media for evaluating alkaline electrolyzer performance through CFD modeling. Renew Energy Focus 2024;49:100575. http://dx.doi.org/10.1016/j.ref.2024.100575.

[18] Liu M, Li S, Shi Y, Cai N. Experimental characterization and non-isothermal simulation of a zero-gap alkaline electrolyser with nickel-iron porous electrode. Int J Hydrog Energy 2024;63:1158–73. http://dx.doi.org/10.1016/j.ijhydene.2024.03.145.

[19] Linares-Solano A, Lillo-Ródenas M, Marco-Lozar J, Kunowsky M, Romero-Anaya A. NaOH and KOH for preparing activated carbons used in energy and environmental applications. Int J Energy Environ Econ 2012;20(4):59–91.

[20] Bideau DL, Mandin P, Benbouzid M, Kim M, Sellier M. Review of necessary thermophysical properties and their sensivities with temperature and electrolyte mass fractions for alkaline water electrolysis multiphysics modelling. Int J Hydrog Energy 2019;44(10):4553–69. http://dx.doi.org/10.1016/j.ijhydene.2018.12.222.

[21] Shreir LL. Corrosion, metal/environment reactions. United Kingdom: Elsevier; 2013.

[22] deGroot M. Alkaline water electrolysis: With or without iron in the electrolyte? Curr Opin Chem Eng 2023;42:100981. http://dx.doi.org/10.1016/j.coche.2023.100981.

[23] Rossum GV, Drake F. Python 3 reference manual. Scotts Valley, CA: CreateSpace; 2009.

[24] An L, Zhao T, Chai Z, Tan P, Zeng L. Mathematical modeling of an anion-exchange membrane water electrolyser for hydrogen production. Int J Hydrogen Energy 2014;39:19869–76. http://dx.doi.org/10.1016/j.ijhydene.2014.10.025.

[25] Raoult's law. 2024, https://en.wikipedia.org/wiki/Raoult%27s_law. [Last Accessed on 15 March 2024].

[26] Falcão D, Pinto A. A review on PEM electrolyzer modelling: Guidelines for beginners. J Clean Prod 2020;261. http://dx.doi.org/10.1016/j.jclepro.2020.121184.

[27] Bove R, Ubertini S. Modeling solide oxide fuel cells. Springer; 2008.

[28] Vidalez AG, Millan N, Bock C. Modeling of anion exchange membrane water electrolyzers: The influence of operating parameters. Chem Eng Res Des 2023;194:636–48. http://dx.doi.org/10.1016/j.cherd.2023.05.004.

[29] Vugrin K, Swiler L, Roberts R, Stucky-Mack N, Sullivan S. Confidence region estimation techniques for nonlinear regression in groundwater flow: Three case studies. Water Resour Res 2007;43. http://dx.doi.org/10.1029/2005WR004804.

[30] Press W, Teukolsky S, Vetterling W, Flannery B. Numerical recipes: The art of scientific computing. Cambridge, UK: Cambridge University Press; 2007.